# A wide-angle X-ray study of the development of molecular orientation in crosslinked natural rubber

**G. R. Mitchell***
*Department of Metallurgy and Materials Science, University of Cambridge, Pembroke Street, Cambridge, CB2 3QZ, UK*
*(Received 17 February 1984)*

Molecular orientation parameters have been measured for the non-crystalline component of crosslinked natural rubber samples deformed in uniaxial tension as a function of the extension ratio and of temperature. The orientation parapeters $\langle P_2(\cos\alpha)\rangle$ and $\langle P_4(\cos\alpha)\rangle$ were obtained by an analysis of the anisotropy of the wide-angle X-ray scattering functions. For the measurements made at high temperatures the level of crystallinity detected was negligible and the orientation–strain behaviour could be compared directly with the predictions of molecular models of rubber elasticity. The molecular orientation behaviour with strain was found to be at variance with the estimates of the affine model particularly at low and moderate strains. Extension of the crosslinked rubber at room temperature led to strain–crystallization and measurements of both the molecular orientation of the non-crystalline chains and the degree of crystallinity during extension and relaxation enabled the role of the crystallites in the deformation process to be considered in detail. The intrinsic birefringence of the non-crystalline component was estimated, through the use of the $\langle P_2(\cos\alpha)\rangle$ values obtained from X-ray scattering measurements, to be $0.20 \pm 0.02$.

**(Keywords: molecular orientation; X-ray scattering; natural rubber; strain crystallization; birefringence; networks)**

## INTRODUCTION

The measurement of the development of molecular orientation in rubber networks with increasing applied strain has traditionally been made by birefringence techniques[1,2]. Such data have been invaluable as qualitative tests of the predictions of deformation models notably those statistical chain models arising from the original work of Kuhn and Grün[3]. However, although birefringence provides a measure of the molecular orientation, the results are difficult to convert to quantitative orientation parameters. Any conversion relies upon an intrinsic birefringence, that is, that which would occur in a perfectly oriented system. This intrinsic birefringence may only be obtained by means of an independent orientation measurement or by calculation based upon rather empirical methods. Within this framework, it is perhaps not surprising that the emphasis in testing predictions of deformation models against experimental data has been upon force–extension curves which are more readily available. This is despite the more direct link that the measurement of chain orientation has with the molecular aspects of the deformation process.

There are many techniques for the quantitative measurement of preferred molecular orientation[4–6], although none appears to have been applied to rubber networks. Wide-angle X-ray scattering (WAXS) is particularly useful since it allows both the orientation parameters and the local structure to be evaluated[7]. This paper presents the results of the application of WAXS techniques to the measurement of molecular orientation parameters in crosslinked natural rubber. The study includes the determination of an intrinsic birefringence which allows earlier optical studies to be re-evaluated on a quantitative basis.

## MEASUREMENT OF MOLECULAR ORIENTATION

For samples subjected to uniaxial tension, as in this study it is only necessary to define the distribution of molecular chain segments about the extension axis. The most convenient method of describing the distribution $D(\alpha)$ of these directors in space is by exploiting the properties of a series of orthogonal functions $P_n(\cos\alpha)$, where $\alpha$ is the angle between the axis of the orienting unit and the extension axis of the specimen, and $P_n$ are Legendre polynomials. For a system with uniaxial and inversion symmetry only the even harmonics are required, and for a sample of low orientation only the first few terms will be significant:

$$\begin{aligned} P_0(\cos\alpha) &= 1 \\ P_2(\cos\alpha) &= (3\cos^2\alpha - 1)/2 \\ P_4(\cos\alpha) &= (35\cos^4\alpha - 30\cos^2\alpha + 3)/8 \end{aligned} \quad (1)$$

$\langle P_2(\cos\alpha)\rangle$ is often referred to as the 'Hermans Orientation function', and the experimental birefringence $\Delta n$ is related to it (assuming a number of conditions hold) by:

$$\Delta n = \langle P_2(\cos\alpha)\rangle \Delta n^0 \quad (2)$$

* Present address: J. J. Thomson Physical Laboratory, University of Reading, Whiteknights, Reading, RG6 2AF, UK.

0032-3861/84/111562-11$03.00

where $\Delta n^0$ is the intrinsic birefringence. The anisotropy in the X-ray scattering pattern at a particular scattering vector $s$†, $I(\alpha)$ may be considered to be the consequence of smearing or convoluting the scattering which would be associated with a single orienting structure $I_u(\alpha)$, with the orientation function $D(\alpha)$:

$$I(\alpha) = I_u(\alpha) * D(\alpha) \tag{3}$$

If these three functions are expressed in terms of their spherical harmonics, then as has been previously described[8] the coefficients of the harmonics are related by:

$$\langle P_{2n}(\cos\alpha)\rangle_I = \langle P_{2n}(\cos\alpha)\rangle_{Iu} \cdot \langle P_{2n}(\cos\alpha)\rangle_D \tag{4}$$

The coefficients $P_{2n}(\cos\alpha)$ may be obtained from the experimental scattering function $I(\alpha)$ by:

$$\langle P_{2n}(\cos\alpha)\rangle_I = \frac{\int_0^{\pi/2} I(\alpha) P_{2n}(\cos\alpha) \sin\alpha \, d\alpha}{\int_0^{\pi/2} I(\alpha) \sin\alpha \, d\alpha} \tag{5}$$

$\langle P_{2n}(\cos\alpha)\rangle_D$ and $\langle P_{2n}(\cos\alpha)\rangle_{Iu}$ are defined by analogous relationships. Thus if either the scattering from a single orienting structure is known, or its harmonic coefficients $\langle P_n(\cos\alpha)\rangle$ in the range of $n$ considered, then the harmonic coefficients of the orientation function $D(\alpha)$ follow as a series of quotients.

Previously in a study of the molecular orientation in deformed polymethylmethacrylate[7,9,10], the scattering of vectors $> 1.5$ Å$^{-1}$ was utilized. This scattering arises solely from correlations within each chain segments, and for PMMA with a persistent conformation extending over 8–10 monomer units, the values of $\langle P_{2n}(\cos\alpha)\rangle_{Iu}$ were relatively high. However, for *cis*-polyisoprene the level of persistent conformation is much less, which together with the delocalization of the backbone rotation angles[11] leads to small values of $\langle P_{2n}(\cos\alpha)\rangle_{Iu}$ rendering the measurement of orientation statistically more difficult. Preliminary calculations suggest a value of $\langle P_2(\cos\alpha)\rangle_{Iu}$ of less than 0.1 for a scattering vector of 3.0 Å$^{-1}$. In other words at that scattering vector the observed anisotropy in the scattering is less than 10% of the anisotropy in the molecular orientation.

In this study of natural rubber the anisotropy of the most intense peak in the scattering pattern at 1.35 Å$^{-1}$ was used. This peak arises from spatial correlations between chain segments[12,13] and intensifies in scattering patterns for aligned samples towards the equator, i.e. normal to the extension axis. The anisotropy of this interchain peak has been used in other studies of the molecular orientation in non-crystalline polymers[14,15] and in liquid crystal systems[16,17]. In those studies the coefficients $\langle P_{2n}(\cos\alpha)\rangle_{Iu}$ used were those appropriate to a crystalline array of infinitely long rods. For such an assemblage the interchain scattering is confined to the equatorial layer. The effects upon the values of $\langle P_{2n}(\cos\alpha)\rangle_{Iu}$ of finite length molecular segments which would smear the equatorial peak parallel to the meridional axis, and of spatial order were neglected or considered to be negligible[16,17]. For a perfect system of aligned rods the value of $\langle P_2(\cos\alpha)\rangle_{Iu}$ relevant to the interchain peak is $-0.5$[8]. Consideration of the effects of molecular length and the volume within which there is orientational correlation gives values in the range $-0.33$ to $-0.45$[13]. The value of $-0.45$ was obtained from a model with an orientational correlation volume of radius 15 Å, while the value of $-0.33$ was derived by considering the orienting unit to be equiaxed. In a highly flexible polymer such as *cis*-polyisoprene we would expect the orienting unit to be a short section of the polymer chain perhaps corresponding to a size the order of a monomer unit. If we convert the experimental value for the characteristic ratio $C_\infty$ for *cis*-polyisoprene of 4.7[19] to a persistent length $a$, by the use of the relationship[20]:

$$C_\infty = [2a/l] - 1 \tag{6}$$

where $l$ is the average bond length, we obtain a value of ~4.3 Å. This suggests that the typical segment length is of the same order as the molecular diameter, in accord with X-ray scattering studies of isotropic samples of natural rubber[11]. Accordingly the value of $-0.33$ for $\langle P_2(\cos\alpha)\rangle_{Iu}$ was used. It is relevant to note, however, that since these 'correction' factors are independent of strain, the shape of the orientation *versus* strain curve will be largely unchanged by any minor variations in these factors.

## EXPERIMENTAL

The material used in this study was natural rubber grade SMR5CV lightly crosslinked with dicumylperoxide, kindly prepared by Claude Hepburn of Loughborough University. The samples for the WAXS measurements were 10 mm wide strips cut from a 3 mm thick sheet. The samples were strained in a purpose built device mounted within an Eulerian cradle, which allowed the extended sample to be rotated in its own plane. The cradle formed part of a symmetrical transmission X-ray diffractometer, equipped with an incident beam monochromator, pinhole collimation and step-scanning facilities which has been described previously[18]. The stretched samples were maintained at fixed temperatures by means of a hot air device controlled by a thermocouple in contact with the sample. Extensions and scattering measurements were made at temperatures of 21°C, 56°C and 75°C. The extension ratio was determined from ink marks inscribed on the sample prior to extension. After each series of experiments, the sample was returned to the unstrained state and the gauge length was measured to determine the level of creep; there was no discernable creep.

The X-ray scattering curve from an isotropic natural rubber sample is shown in *Figure 1*. There are peaks at $s \sim 1.35$ Å$^{-1}$ and 3.0 Å$^{-1}$. The minor peak at $s \sim 2.1$ Å$^{-1}$ is associated with a small level of crystalline impurity and its intensity may be used to normalize the scattering for measurements of the level of crystallinity in rubber samples of differing thickness. The scattering

† Where $s = 4\pi \sin\theta/\lambda$.

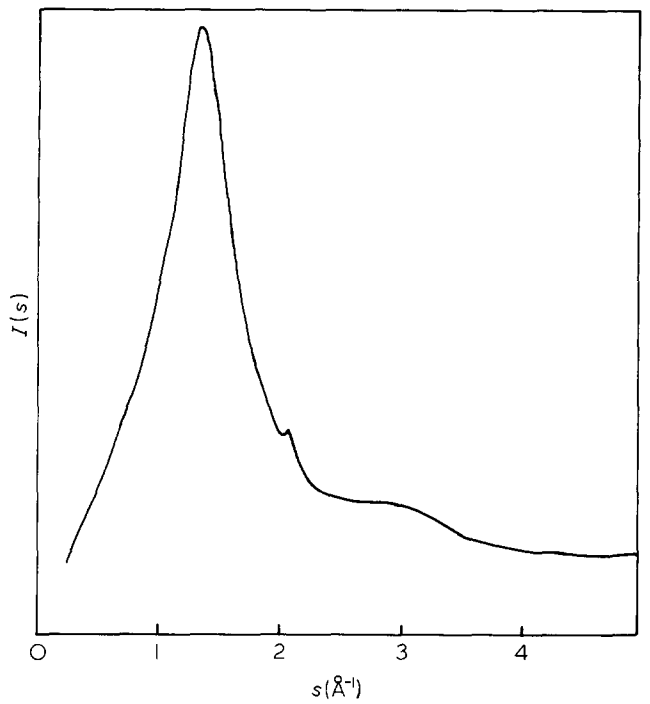


**Figure 1** X-ray scattering intensity function $I(s)$ for an undeformed sample of natural rubber used in this study. The measurements were made at 21°C. $s=4\pi\sin\theta/\lambda$ where $2\theta$ is the angle between the incident and scattered directions

curve is similar in basic form to other non-crystalline polymers[12] and the peak at $s\sim1.35$ Å$^{-1}$ may be associated with spatial correlations between chain segments, while peaks in the scattering curve at $s>2.0$ Å$^{-1}$ are related to correlations within a single chain segment. The local structure of the isotropic material has been considered in depth elsewhere[11], however it is pertinent to report here that the local conformation was determined to be highly irregular with no evidence for any particular level of interchain orientational correlation.

Three types of X-ray scattering data measurements were made.

(a) In order to measure the molecular orientation parameters the anisotropy of the interchain peak at $s\sim1.35$ Å$^{-1}$ was utilized, and the function $I(\alpha)$ was measured over the range $\alpha=0°$ to 90° in steps of $\Delta\alpha=9°$. The air-scattered background was estimated by measuring the intensity at the same value of $s$ but with a sample of equivalent thickness placed in front of the X-ray detector. From an intensity curve normalized in electron units and the theoretical incoherent scattering function[21], the incoherent background was estimated to be ~2% of the measured signal. However, variations in the value of this isotropic background, or the air scatter had no effect upon the values of molecular orientation parameters determined within the level of precision reported in this work. The orientation parameters $\langle P_2\rangle$ and $\langle P_4\rangle$ were obtained after subtraction of this background through the use of equations (4) and (5).

(b) To determine the degree of crystallinity in the extended samples, scans of the scattered intensities were made at fixed $\alpha=90°$ using steps of $0.2°2\theta$. An approximate level of crystallinity was determined from these scans by the use of the relationship:

$$\%\,\text{crystallinity}=\left[1-\frac{I'(s)}{I''(s)}\right]\times 100 \qquad (7)$$

where $I''(s)$ is the scattering from a totally non-crystalline sample and $I'(s)$ is the scattering from the non-crystalline component of a semi-crystalline material. The intensity value $I(s)$ corresponding to the interchain peak at $s\sim1.35$ Å$^{-1}$ was used for these measurements and it was normalized to take account of the thickness variations using the intensity of the impurity peak at $s\sim2.1$ Å$^{-1}$ which had an isotropic distribution.

(c) To monitor the general structure and the crystallite orientation in particular, the complete pattern $I(s,\alpha)$ was recorded over the range $s=0.21$ to 5.0 Å$^{-1}$ in steps of 1° $2\theta$, and $\alpha=0°$ to 90° in steps of 9°. This scattering function will be displayed as an $s$-weighted reduced intensity function $si(s,\alpha)$, the correction and normalization procedures being as used previously[18].

It was observed, as in previous studies[22,23] that the crystallite orientation in the room temperature extended samples was nearly perfectly aligned with the extension axis. This observation enabled the crystalline scattering component to be removed from the function $I(\alpha)$ by extrapolation. As a result the orientation of the *non-crystalline* component *alone* was obtained. The extrapolation procedure is illustrated in *Figure 2*, which shows the azimuthal profile $I(\alpha)$ for $s\sim1.35$ Å$^{-1}$ for a sample with an extension ratio of 4. For measurements made at elevated temperatures it was only for the most highly extended samples, in which a low level of crystallinity

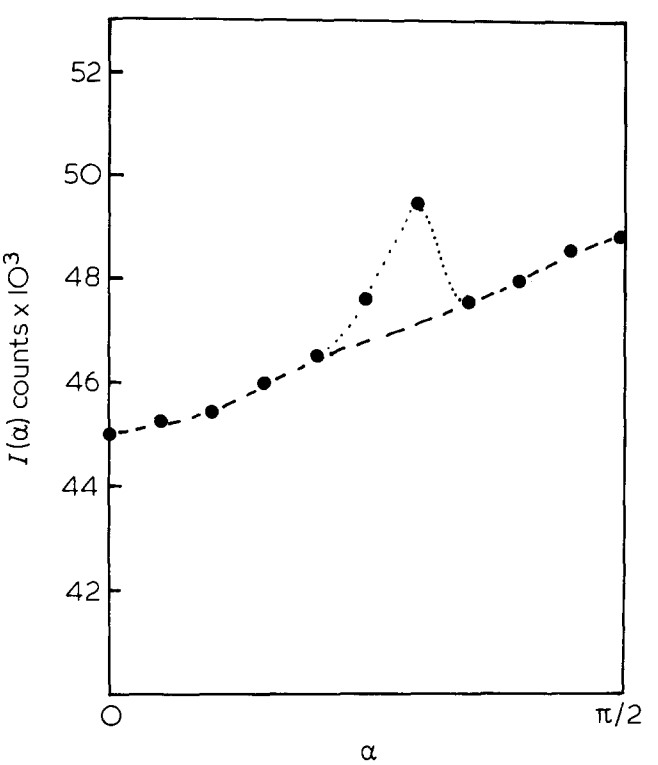


**Figure 2** A plot of the intensity function $I(\alpha)$ for $s=1.35$ Å$^{-1}$ for a sample of natural rubber extended at 21°C with an extension ratio of 4. The filled cirles are the measured data points, and the dashed line represents the extrapolated function used to determine the orientation parameters of the non-crystalline component. The dotted line indicates the contribution from the crystalline fraction

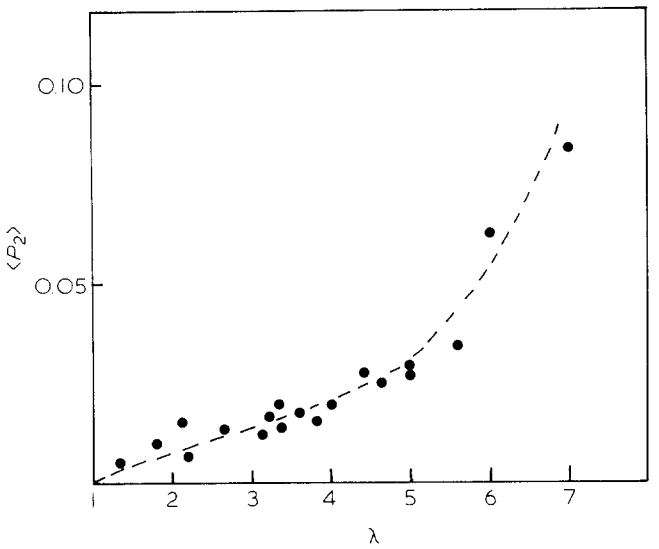


**Figure 3** A plot of the coefficient $\langle P_2 \rangle$ of the orientation distribution function for the *non-crystalline* component of natural rubber extended at 21°C as a function of the extension ratio $\lambda$

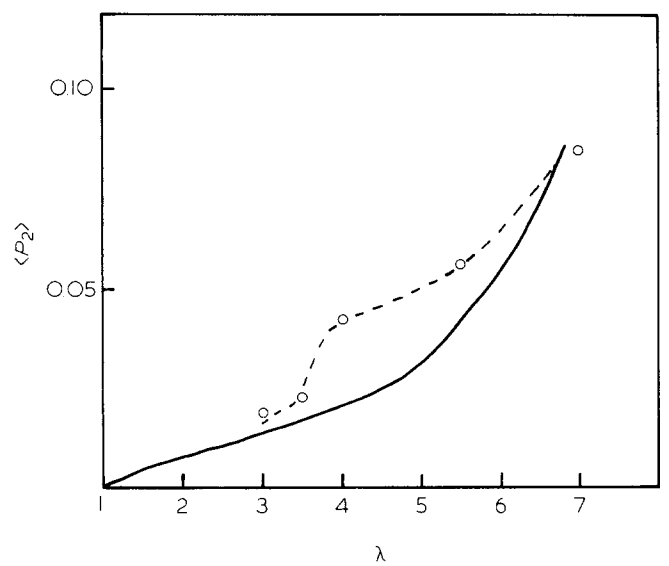


**Figure 4** $\langle P_2 \rangle$ values obtained for the non-crystalline component of natural rubber at 21°C upon unloading in stages a sample previously extended to a maximum strain of $\lambda = 7$. The solid line represents the values obtained on loading, taken from *Figure 3*

was detected, that the above procedure was necessary. The birefringence was measured using quartz wedges and a five order Berek compensator mounted in a transmission light microscope. The modulus of the natural rubber samples was determined using an Instron Tensometer with a strain rate of $10^{-2}\,s^{-1}$. An initial modulus ($E$) was determined with a value of 0.30 MPa. The evaluation of the modulus in terms of the molecular weight between junction points depends upon the precise model of rubber elasticity assumed. In this study we used the modulus determined from the initial slope in the force-extension curve together with the affine model[1] to gain an appreciation of the molecular weight via the relationship:

$$\text{Molecular weight of chain} = 3\rho\, kT/E \qquad (8)$$

with $\rho$ the macroscopic density. This formulation gives a molecular weight of ~23600, a value broadly comparable with that calculated on the basis of the quantity of dicumyl-peroxide used and its efficiency of crosslinking[24].

## RESULTS

### *Extension at 21°C*

*Figure 3* shows the values of $\langle P_2 \rangle$ obtained for extensions at 21°C in the range of $\lambda = 1$ to 7. The values of $\langle P_4 \rangle$ measured were, within the experimental error, zero over the complete strain range considered here. The $\langle P_2 \rangle$ *versys* $\lambda$ curve shows the characteristic shape with its pronounced curvature, traditionally associated with orientation development in rubbers. There is an approximately linear relationship between $\langle P_2 \rangle$ and $\lambda$ from $\lambda = 1$ to 4.5, followed by an increasingly steeper upturn. It is emphasized that the $\langle P_2 \rangle$ values shown for the *non-crystalline* component of the material. *Figure 4* shows the values of $\langle P_2 \rangle$ for the non-crystalline component obtained upon unloading in stages a sample previously strained to $\lambda = 7$. There is a significant departure in the curve for $\lambda > 3$ from the values of $\langle P_2 \rangle$ obtained in the loading cycle. The levels of crystallinity determined from the scattering measurements using equation (7) are shown in *Figure 5* for both the loading and unloading cycles. There is again a marked hysteresis similar to that observed in the $\langle P_2 \rangle$ *versus* $\lambda$ plot (*Figure 4*). A completely non-crystalline sample is only obtained by unloading to $\lambda = 2$. To illustrate the nature of the crystallite orientation, *Figures 6* and *7* show the $s$-weighted reduced intensity functions $si(s,\alpha)$ for the samples extended to $\lambda = 7$ and $\lambda = 4.4$ at 21°C. In the highly extended sample (*Figure 6*) the crystalline component dominates the scattering function. The

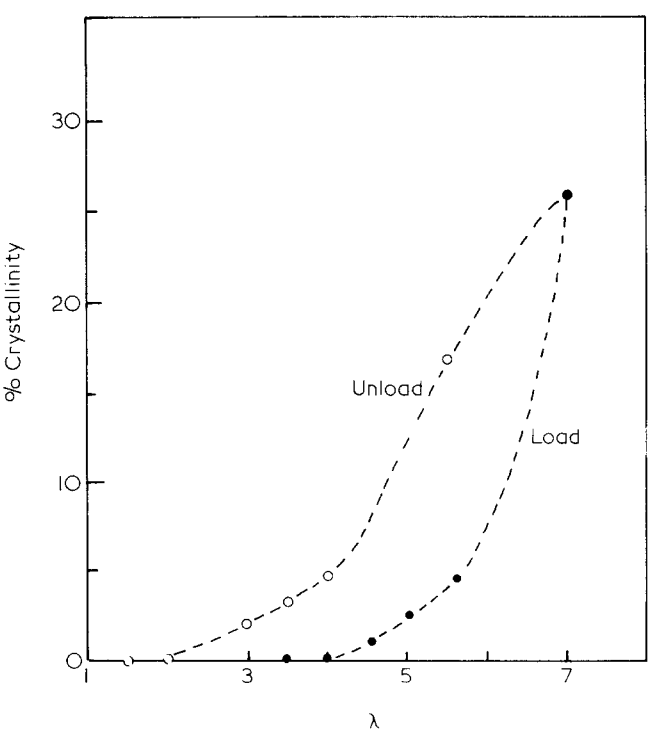


**Figure 5** A plot of the %crystallinity evaluated from the X-ray scattering curves using equation (7), as a function of the extension ratio, for both the loading (filled circles) and unloading (open circles) cycles at 21°C

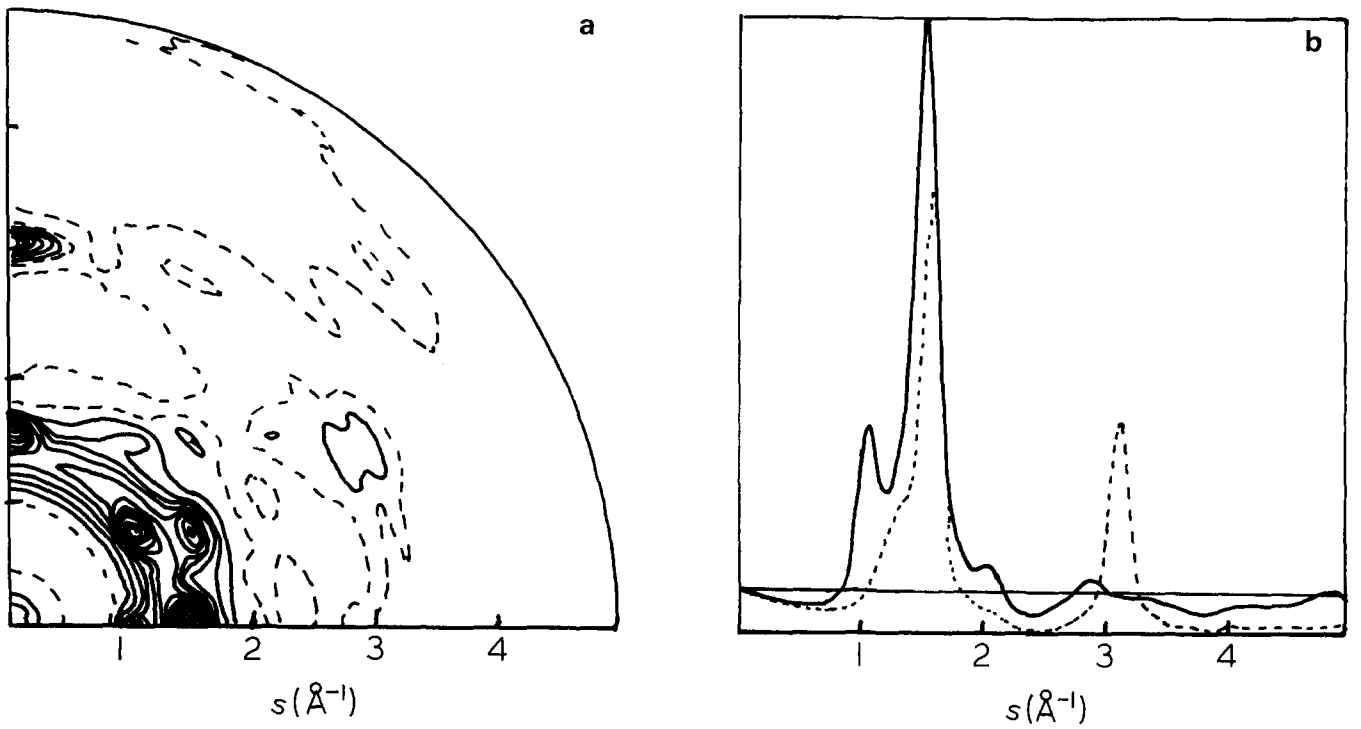


**Figure 6** (a) The scattering function $si(s,\alpha)$ for a natural rubber sample deformed at 21°C with an extension ratio of 7. The extension axis is vertical, and the broken contours indicate negative values. (b) The equatorial ($\alpha=90°$, solid line) and the meridional ($\alpha=0°$, broken line) sections of the intensity surface shown in *Figure 6a*

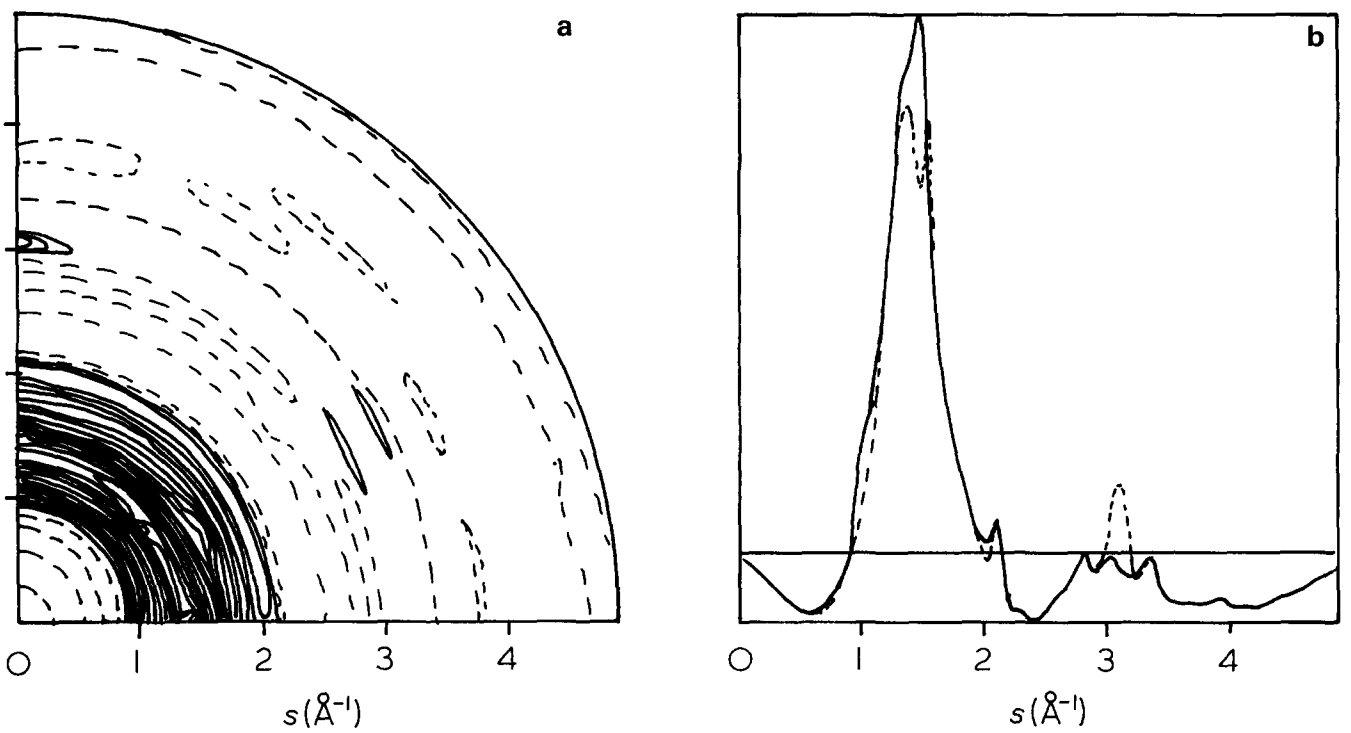


**Figure 7** (a) The scattering function $si(s,\alpha)$ for a sample of natural rubber deformed at 21°C with an extension ratio of 4.4. (b) The equatorial and meridional sections of the intensity surface of *Figure 7a* (key as for *Figure 6b*)

arcing of the crystalline diffraction spots is extremely limited, indicating a high level of crystallite orientation. The degree of crystallinity in the sample with $\lambda=4.4$ (*Figure 7*) is small and it is difficult to identify the crystal diffraction maxima against the broad non-crystalline scattering peaks. If the isotropic component of the scattering which, considering the low level of orientation will be effectively the non-crystalline component, is subtracted from the scattering function the remaining anisotropic part or principally the crystalline scattering is revealed in more detail. *Figure 8* shows the result of the subtraction; the anisotropic component[25] for the

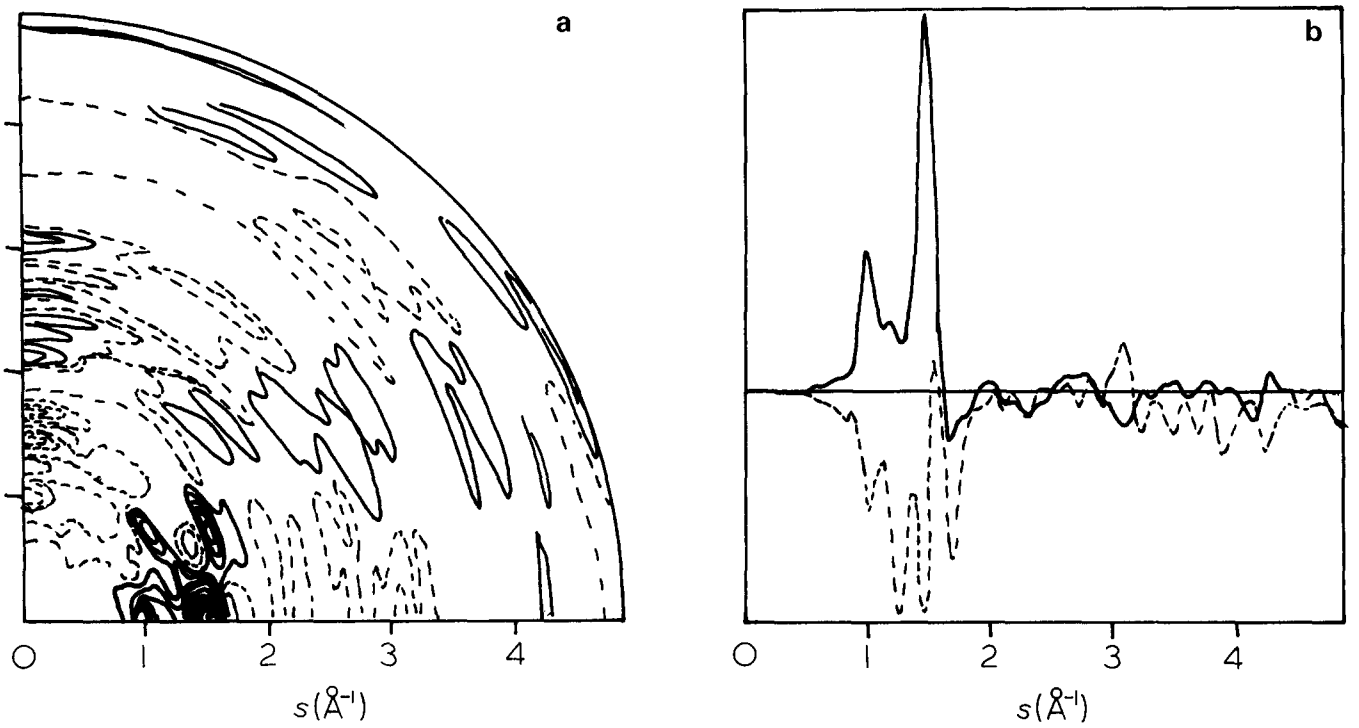


**Figure 8** (a) Scattering function $si'(s,\alpha)$ corresponding to that shown in *Figure 7a* from which the isotropic component $\int_0^{\pi/2} si(s,\alpha) \sin\alpha \, d\alpha$ has been subtracted to illustrate the high level of crystalline orientation. (b) The equatorial and meridional sections of *Figure 8a* (key as for *Figure 6b*)

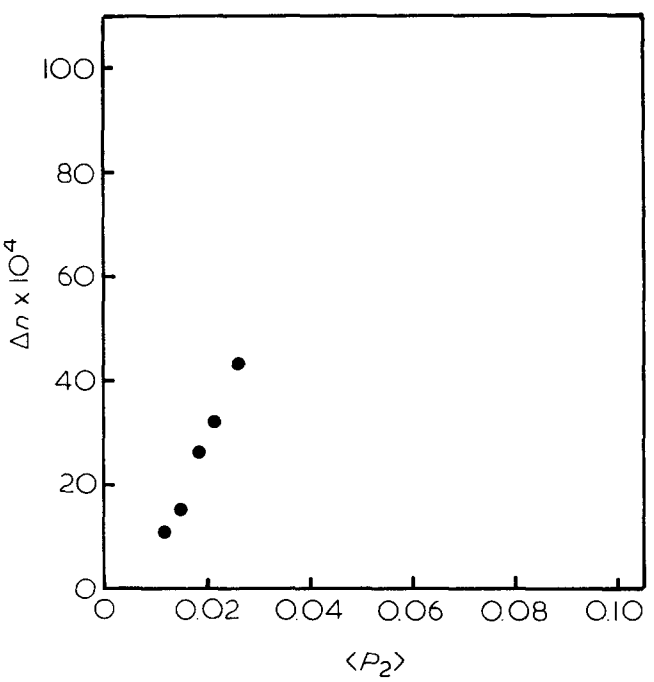


**Figure 9** Plot of the measured birefringence $\Omega n$ against the orientation parameter $\langle P_2 \rangle$ obtained from the WAXS analysis. The slope gives the intrinsic birefringence $\Omega n^\circ$

sample with $\lambda = 4.4$ exhibits a comparable level of arcing of the crystalline diffraction maxima to that seen for the highly extended sample.

*Intrinsic birefringence*

It is clear from the scattering studies of the sample extended at 21°C, that there is significant crystallization for $\lambda > 4$. Birefringence experiments are unable to distinguish between the effects of orientation in the crystalline and non-crystalline regions. Thus to enable the intrinsic birefringence of the non-crystalline network alone to be obtained, measurements were restricted to values of $\lambda < 4.5$ The birefringence determinations were performed on the X-ray samples using the same tensometer as used for the scattering studies. *Figure 9* shows a plot of the birefringence values measured for values of $\lambda < 4.5$ and the equivalent $\langle P_2 \rangle$ components of the orientation distribution functions obtained using the WAXS techniques described above. There is a reasonable linear relationship, from which, using equation (2) an intrinsic birefringence of $0.2 \mp 0.02$ may be obtained.

*Extension at 56°C and 75°C*

Orientation measurements were made at elevated temperatures in order to suppress the onset of crystallization. However, a small degree of crystallinity was detected in the highly extended samples at 56°C as shown in *Figure 11*. It was found that samples extended at 75°C for $\lambda > 5$ fractured, presumably in part due to thermal degradation. However, the increased temperature would suppress crystallization even at the higher strains, and hence the well-known reinforcing nature of the crystallites would be lost leading to breakage. Accordingly, for the $\lambda > 5$ the values of $\langle P_2 \rangle$ obtained upon extension at 56°C were utilized. *Figure 10* shows the orientation development with increasing strain for the two temperatures. The $\langle P_2 \rangle$ *versus* curve is almost linear over the complete strain range. As for the measurements made at room temperature, the values of $\langle P_4 \rangle$ recorded at 56°C and 75°C were not significantly non-zero.

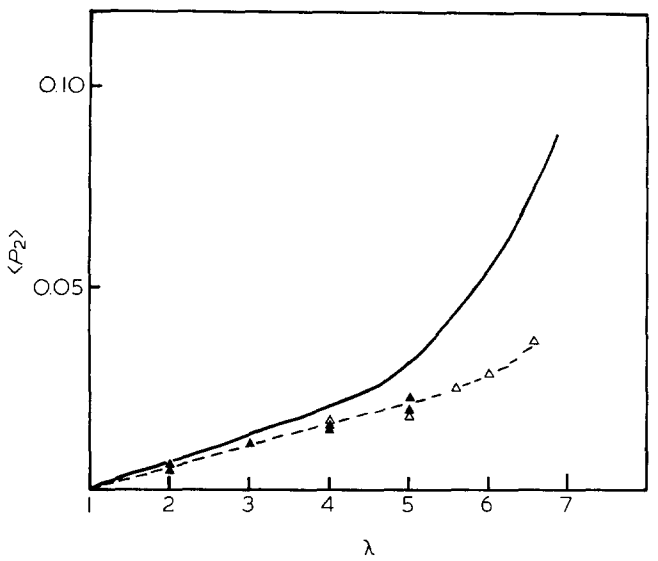


**Figure 10** Plot of the coefficients $\langle P_2 \rangle$ of the orientation function for the non-crystalline component of natural rubber extended at 56°C (open triangles) and 75°C (filled triangles) as a function of the extension ratio $\lambda$. The solid line represents the values of $\langle P_2 \rangle$ obtained for extension at 21°C (from *Figure 3*). The level of crystallinity for the samples at 56°C was zero for $\lambda < 5$

## DISCUSSION

*Predicted orientation–strain behaviour*

The next step is to compare the development of orientation of the non-crystalline component on extension determined by experiment with the predictions of possible molecular models. The classic model of rubber elasticity relates to a network of chains in which the stress is transmitted to the molecular chains only via the junction points. The junction points, or the end-to-end vectors of the chains in the network are considered to deform affinely, that is as if fixed to the macroscopic continuum[1,3]. The rate of development of segmental orientation with applied strain is related to the number of statistical links or segments in the chain between junction points. For small strains it is adequate to assume a Gaussian distribution of chain segments[3,26], but for large strains non-Gaussian distributions are necessary[27,28]. In these models the chains have no interactions except through the junction points. Alternative treatments consider the fluctuations of the junction points[29] about their mean positions in the network, which leads to non-affine behaviour of the chain vectors[30]. Such so-called phantom chain models differ in their predictions of stress and orientation[31] from the affine model by a factor of one half. More recently the effects of neighbouring chains have been introduced into the phantom chain model[31–33], although their interactions are assumed only to apply to the constraints upon the locations of junction points. Such a model predicts an additional strain dependent term to the phantom chain model which leads to greater initial rates of molecular orientation with strain[31]. We may consider these models to lie in a spectrum of behaviour with the affine and phantom chain models providing the limiting cases. Intermolecular interactions have been introduced more explicitly into network models by several studies[34–36], involving short-range orientational coupling between adjacent chain segments. These interactions also increase the chain orientation, although are thought[34] to have little effect upon the stress–strain behaviour. More radical approaches have been considered by Kilian[37] and by Brown and Windle[38], although the former does not directly consider orientational behaviour. Brown *et al.*[38] separate out the response of the material to stress, into orientational and translational components, an approach which provides an adequate fit to the stress–orientational strain data relating to thermoplastic polymers deformed above $T_g$. They do not apply the model to natural rubber or comparable systems.

In the first instance, we shall adopt the formulation of Nobbs and Bower[28] which uses Treloar's expansion of the inverse Langevin function[27] to predict the orientational behaviour of an affine non-Gaussian chain model. The only parameter is $n$, the number of statistical links or segments between junction points. *Figure 12* shows the development of $\langle P_2 \rangle$ with strain predicted by the affine model for a range of $n$. The values of $n$ were chosen to provide $\langle P_2 \rangle$ levels which embraced those observed. Similar curves may be calculated for the phantom chain model, in which case the equivalent values of $n$ will be half those indicated, although for the phantom chain model the distribution of chain segments is assumed to be Gaussian. It is noticeable that there is a greater similarity in the shape of the curve for measurements made at 21°C to the predicted relationships, than for the curve representing the high temperature experiments. If we equate a statistical link with a monomer in line with the scattering studies[11], the molecular weight obtained from the initial modulus (equation (8)) indicates a value for $n$ of ~350. Before attempting to refine the molecular model to predict curves in better agreement with the

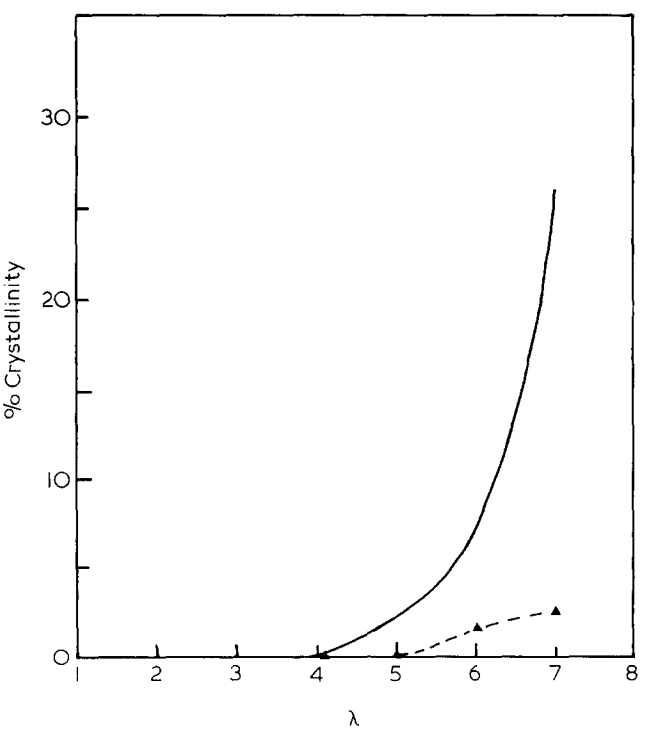


**Figure 11** %Crystallinity measured for samples of natural rubber extended at 56°C (filled triangles) as a function of the extension ratio $\lambda$. The solid line represents the crystallinity measured for samples extended at 21°C (*Figure 5*)

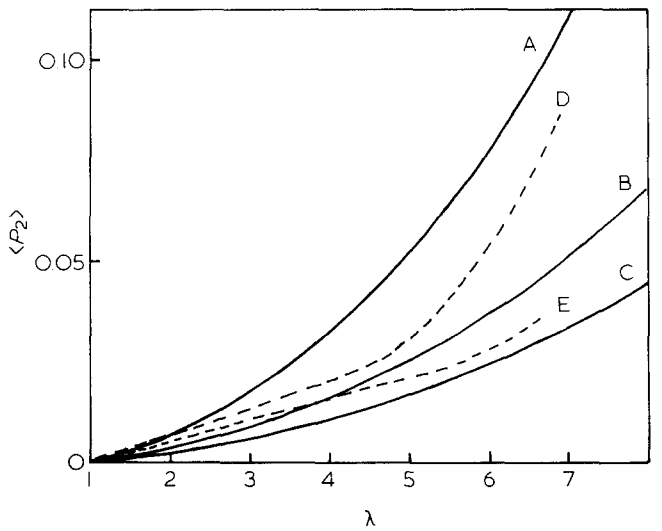


**Figure 12** Comparison of the predicted orientation behaviour of the affine model for a range of $n$, the number of statistical links between junction points (A) $n=100$, (B) $n=200$, (C) $n=300$, with the experimentally determined $\langle P_2 \rangle$ values obtained for extensions at (D) 21°C and (E) 56°C and 75°C

experimental values, it is more relevant to consider the reasons for the differences between the orientational behaviour observed at different temperatures.

*Effect of crystallization*

It is well known that natural rubber crystallizes upon the application of stress at room temperature, and the phenomenon has been extensively studied (for example refs. 22, 23, 39). The development of crystallinity with strain observed in this work (*Figure 5*) is in accord with those obtained previously[23,40-42], in particular the onset of crystallinity at $\lambda \sim 3.5$ and a limiting level of crystallinity at high strains of $\sim 30\%$[23]. As has been previously noted for natural rubber[22,39] and in studies of molten networks of polyethylene[43,44] the level of crystalline orientation is particularly high even at low strains. This is in marked contrast to the small degree of preferred orientation in the non-crystalline component. It is also apparent that the level of molecular orientation in the non-crystalline component as indicated in *Figure 3*, accelerates as the degree of crystallinity exceeds 2–3%. It is emphasized again that the $\langle P_2 \rangle$ values obtained in this work relate to the *non-crystalline* component *alone*, unlike the more traditional birefringence measurements. Thus the marked acceleration in the development of molecular orientation (*Figure 3*) is not a measure of the preferred alignment of the crystallites, although the effect is clearly associated with the onset of crystallinity. Such an identification is manifestly supported by the absence of a similar upturn in the $\langle P_2 \rangle$ *versus* strain curve relevant to the higher temperature measurements, for which, even at the highest strains, the crystallinity levels measured were particularly small (*Figure 11*).

It is commonly thought that the crystallites act as crosslinks, resulting in a decrease in the effective molecular weight between junction points (and thus of $n$) with increasing strain. This will naturally result in an accelerating enhancement of the orientation with strain. However, we should also note that as the crystallites are almost perfectly aligned with respect to the extension axis, they therefore cannot accommodate further strain by orientation. In effect the active volume of the material has been reduced, resulting in a higher effective strain upon the non-crystalline fraction. If the crystallites are equiaxed we can postulate an effective strain $\lambda'$, of the form:

$$\lambda' = \lambda \left[ \frac{1}{1-f} \right]^{1/3} \tag{9}$$

where $f$ is the fraction of crystalline material and $\lambda$ is the strain with respect to the sample volume. Using the values of crystallinity measured from the scattering curves (*Figure 5*), we calculate the $\langle P_2 \rangle$ *versus* $\lambda'$ curve shown in *Figure 13* for extensions made at room temperature. The solid line indicates the observed behaviour, the broken line the corrected curve using equation (9). Naturally the effects of the correction are most marked at large strains where the levels of crystallinity are highest. For values of $\lambda < 5$ the curves are identical. The corrected curve for the $\langle P_2 \rangle$ values obtained at the highest temperatures is not shown since the small levels of crystallinity detected (less than 3%) do not significantly effect $\lambda'$. However, even with this modification the orientational behaviour at 21°C is still considerably different to that observed at the higher temperatures: there remains an accelerating upturn in the $\langle P_2 \rangle$ *versus* $\lambda$ curve.

The breadths of the crystalline diffraction spots suggest a crystallite size of $\sim 50$ Å, and we can utilize this size to estimate the spacing of the crystallites in the deformed material. If the crystallites are dispersed randomly throughout the sample, the crystallinity level of 3% for $\lambda = 5$ would be equivalent to a crystallite spacing of 160 Å, and for 26% crystalline ($\lambda = 7$), the crystallite separation would be 75–80 Å. These values may be compared with the average junction separation of $\sim 200$ Å in the isotropic state for a chain of molecular weight of 23 600 and $C_\infty = 4.7$. Alternatively the crystallite separation of 80 Å would correspond to a chain

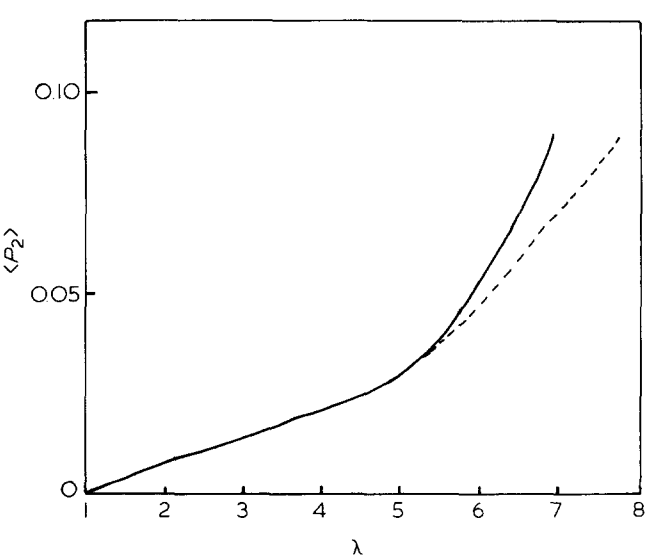


**Figure 13** A plot showing the $\langle P_2 \rangle$ *versus* $\lambda$ curve obtained for extensions at 21°C (full line) and the modified curve (broken line) taking account of the reducing active volume of the sample due to the increasing levels of highly oriented crystallites with applied strain, using equation (9)

contour length equivalent to ~55 statistical links. Hence the linear distances of the crystallites from each other and from the conventional junction points are considerably less than that calculated from the initial crosslink density. The results of these calculations support the proposals that part of the increasing rate of orientation is due to the crystallites, which form as a result of the applied strain, acting as junction points. A similar effect is seen in the orientation behaviour upon unloading. The maintenance of a high level of crystallinity on unloading a sample to reduced strains (*Figure 5*), results in enhanced $\langle P_2 \rangle$ values, significantly higher than the equivalent $\langle P_2 \rangle$ values obtained on loading. This behaviour leads to a hysteresis loop in the orientation–strain curve, as found by Treloar[26] with birefringence–strain measurements. Equivalence between the unloading and loading cycles is only reached when the %crystallinity has dropped to ~3%. This is a similar value to that observed at the point in the loading cycle when the upturn in the $\langle P_2 \rangle$ curve is initiated. Following the calculations of the crystallite separation above this particular level of crystallinity corresponds to an inter-crystallite distance of 160 Å or approximately the same order as that for the mean inter-junction distance in the isotropic state, although of course the average separation between crosslinks and crystallites will be much less. The crystallites may differ in their actions as crosslinks to the normal chemical junction points. Firstly they represent an inhomogeneous distribution of effective junction points, segregated into small volumes and this could lead to inhomogeneous deformation behaviour. Secondly, they may be more constrained within the network due to this segregation, and the orientation behaviour of the chain vectors could approach that of the affine model rather than the phantom chain system, in which junction points are exposed to large fluctuations[33]. Thus we may qualitatively account for the difference between the high-temperature and room-temperature orientational behaviour at large strains by the onset of crystallization which increases *both* the effective strain upon the non-crystalline component, and the crosslink density.

However, such proposals do not accommodate the differences observed at low and moderate strains. It has been suggested[42], that highly defective crystallite-like entities are formed at low strains prior to the onset of true crystallization, and act as nuclei for the formation of crystallites at higher strains. As described earlier several treatments of rubber elasticity[34–36] have attempted to include some local orientational interactions between chain segments. Such interactions would naturally be highly susceptible to variations in temperature, and it is interesting to note that significant temperature effects have been observed in the orientational behaviour of poly(methylmethacrylate) at temperatures above $T_g$[9,45], although a-PMMA is a non-crystallizable polymer. It is worthwhile to record that from the breadths of the diffraction maxima, the crystallite size does not appear to increase significantly with increasing strain. It is not the intention to speculate on the various theories (for example see refs. 46–48) of strain crystallization, but it is clear from the disparate levels of molecular orientation in the crystalline and non-crystalline regions, that crystallization must involve appreciable growth from small particularly well aligned nuclei.

*High temperature behaviour*

We shall now turn attention to the orientational behaviour observed for extensions at 56°C and 75°C. It is now clear that the accelerating orientational behaviour observed at room temperature generally associated with the simple affine model is concerned with the onset of crystallization. No upturn is observed for the higher temperature measurements, for which no crystallinity was detected. In fact there is a slight suggestion of the start of a turn up in *Figure 10* at $\lambda \sim 6.5$, and this may be related to the small level of crystallinity detected at this strain as indicated in *Figure 11a*.

*Comparison of the* $\langle P_2 \rangle$ values observed at 56°C and 75°C with the predicted behaviour for the affine model is poor (*Figure 12*). It would appear that the rate of orientation development at low strains is greater than predicted by the affine model. This type of behaviour is in accord with the predictions of the modified phantom chain model proposed by Erman and Flory[31]. However, such enhancement of the molecular orientation is also predicted by those models[34–36] with more specific local intermolecular interactions and presumably also by those models which postulate a significant role for entanglements[49,50]. A study of the effects on orientational behaviour with strain of variations of both temperature and crosslink density should help to distinguish between these proposals. At higher strains there is no evidence for an upturn related to the finite extensibility of the network proposed by Smith *et al.*[40,41], although since the level of crosslinking is low the limiting strain, $\sqrt{n}$, will be in the range $\lambda \sim 14$–18. At room temperature the upturn in the $\langle P_2 \rangle$ *versus* $\lambda$ curve may be attributed to the onset of crystallization as proposed by Flory[30] and Mark[51].

*Optical studies*

Although birefringence is a simple and convenient method of evaluating molecular orientation, its relationship to the molecular structure is unclear. Under some circumstances intermolecular effects may be as important as the anisotropic polarizability of an individual molecular segment[52]. Equally important may be the effects of stress birefringence, widely used in photoelastic stress analysis. For several polymers a linear relationship has been established between the birefringence and values of molecular orientation measured by WAXS techniques[45] or spectroscopic methods (for example see ref. 53). However, such measurements have been made for glassy polymer samples in which the molecular orientation has been frozen in by rapid quenching, and thus the samples are not directly under load during the birefringence measurements. In these circumstances the level of stress birefringence would be considerably less although not necessarily zero. For natural rubber the attainment of linearity over a wide range of strain at room temperature is prevented by the onset of crystallization. The measurements presented in *Figure 9* represent the first step in establishing a reliable intrinsic birefringence which enables optical measure-

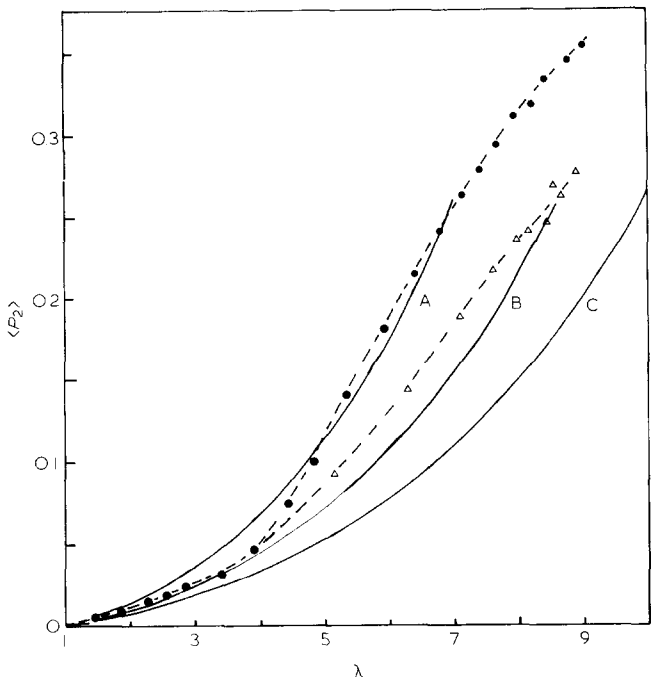


**Figure 14** $\langle P_2 \rangle$ values obtained from the birefringence results of Treloar[26] through the use of equation (2) and an intrinsic birefringence $\Omega n^\circ$ of 0.20. The filled circles are for extension at 25°C and the open triangles for extension at 75°C. The solid lines are the predictions of the affine model for (A) $n=50$, (B) $n=75$ and (C) $n=100$

ments to be normalized independently to provide quantitative orientation measurements. The value obtained in this work of $\Delta n^\circ = 0.20 \pm 0.02$ is lower than that proposed originally by Treloar[26] of 0.28. However, if the segmental anisotropy determined by Morgan and Treloar[54] is converted to an intrinsic birefringence, a value of 0.19 is obtained, which is in particularly good agreement with that obtained in the current study.

The estimate of $\Delta n^\circ$ enables the birefringence results of earlier studies to be re-evaluated on an absolute basis. As an example, *Figure 14* shows the birefringence results of Treloar[26] converted to $\langle P_2 \rangle$ values through the use of equation (2), and the value of $\Delta n^\circ$ of 0.2. From the original Figure[26] it is not possible to differentiate at low strains the values appropriate to 75°C, but the general trends are clear, and the experimental curves are compared to the predictions of the affine model for a range of $n$. From hysteresis in the birefringence curves, Treloar related the departure of the room-temperature data from the predicted behaviour to the effects of crystallinity. The curve for the room temperature measurements (*Figure 14*) is similar in shape to that measured in this work (*Figure 3*). However, the $\langle P_2 \rangle$ values from the birefringence measurements are much higher due to the inclusion of the crystallite orientation, which could be separated out in the WAXS studies. Although Treloar[26] detected no hysteresis in the stress–birefringence behaviour for samples extended at 75°C and above, he suggests from hysteresis in the strain–birefringence data that, even at 100°C, some crystallinity may be present. The initial modulus measurements of Treloar suggest a value of $n \sim 90$ (a much higher crosslink density than used in this study), which would provide predicted $\langle P_2 \rangle$ values in approximate accord with the magnitudes of the experimental $P_2$ parameters. However, there is poor agreement between experiment and theory in terms of the shape of the $\langle P_2 \rangle$ *versus* strain curve, as has already been observed with the orientational behaviour using WAXS techniques.

*Summary*

It is clear that the deformation behaviour of crosslinked natural rubber at room temperature is particularly complex. Any successful theory of strain crystallization must not only take account of the formation of the crystallites from well oriented nuclei and their subsequent growth, but also the distortion of the chains in the remaining non-crystalline component. The apparent match between experimental orientation behaviour at room temperature and the predictions of the affine model is due to the onset of crystallization. Thus data used in this manner should be treated with caution unless the levels of crystallinity have been determined. However, reliable data can be obtained at higher temperatures where crystallinity has been suppressed. Orientation parameters obtained in this way show the simple affine model to require modification particularly for low and moderate strains. Possible modifications to the affine model relevant to natural rubber but considered within the context of a range of polymers are discussed elsewhere[55].

## CONCLUSIONS

(a) Careful analysis of the anisotropy in the wide-angle X-ray scattering patterns from extended samples provides a useful and relatively straightforward method for obtaining quantitative orientation parameters $\langle P_2 \rangle$ and $\langle P_4 \rangle$ for rubber networks as a function of strain.

(b) The nature of the crystallite morphology in the extended natural rubber samples enables the molecular orientation of the crystalline and non-crystalline components to be evaluated separately.

(c) The X-ray scattering technique is particularly useful as it also enables the levels of crystallinity and other structural changes to be monitored concurrently with the orientation measurements.

(d) Comparison of the experimentally determined chain orientation parameters $\langle P_2 \rangle$ with those predicted for the affine model indicate that the agreement previously suggested is only observed for a network containing some crystallinity, which affects the orientational behaviour of the non-crystalline chains.

(e) Measurements of the molecular orientation at higher temperatures where crystallinity has been suppressed, are at variance with the predictions of the affine model, particularly at low and moderate strains.

(f) Parallel measurements of the birefringence and molecular orientation parameters using WAXS techniques provide an estimate of the intrinsic birefringence of non-crystalline natural rubber of $0.02 \pm 0.02$.

## ACKNOWLEDGEMENTS

The particular contribution of Claude Hepburn of Loughborough University in preparing the crosslinked samples is gratefully acknowledged. The author wishes to thank Philip Lamb for the modulus measurements, and David Brown and Alan Windle for their interest and encouragement, and also SERC for the provision of funding.

## REFERENCES


1 Treloar, L. R. G. 'The Physics of Rubber Elasticity', (3rd Edn.), Oxford University Press, London, 1975
2 Dusec, K. and Prins, W. *Adv. Polym. Sci.* 1969, **6**, 1
3 Kuhn, W. and Grün, H. *Kolloid Z.* 1942, **101**, 248
4 Read, B. E. in 'Structure and Properties of Oriented Polymers', (Ed. I. M. Ward), Applied Science, London, 1975, Ch. 4
5 Ward, I. M. *J. Polym. Sci. Polym. Symp. Edn.* 1977, **58**, 1
6 Kawai, H. and Nomura, S. in 'Developments in Polymer Characterisation 4', (Ed. J. V. Dawkins), Applied Science, London, 1983, Ch. 6
7 Mitchell, G. R. and Windle, A. H. *Polymer* 1983, **24**, 285
8 Lovell, R. and Mitchell, G. R. *Acta Crystallogr.* 1981, **A37**, 135
9 Mitchell, G. R., Pick, M. and Windle, A. H. *Polymer* 1983, **24** (*Commun.*), 16
10 Brown, D. J. and Mitchell, G. R. *J. Polym. Sci. Polym. Lett. Edn.* 1983, **21**, 341
11 Mitchell, G. R. in preparation
12 Lovell, R., Mitchell, G. R. and Windle, A. H. *Faraday Disc.* 1980, **68**, 46
13 Mitchell, G. R. to be submitted to *Colloid Polym. Sci.*
14 Wilchinsky, Z. W. *J. Polym. Sci. A-2* 1968, **6**, 281
15 Biangardi, H. J. *J. Polym. Sci. Polym. Phys. Edn.* 1980, **18**, 903
16 Mitchell, G. R. and Windle, A. H. *Polymer* 1983, **24**, 1513
17 Leadbetter, A. J. and Wrighton, P. G. *J. Phys. (Paris) Colloq.* 1979, **37**, 3C–234
18 Mitchell, G. R. and Windle, A. H. *Colloid Polym. Sci.* 1982, **260**, 754
19 Mark, J. E. *J. Am. Chem. Soc.* 1966, **88**, 4354
20 Flory, P. J. 'Statistical Mechanics of Chain Molecules', Wiley–Interscience, New York, 1969
21 International Tables for X-ray Crystallography, Vol. IV, Kynoch Press, Birmingham, 1974
22 Luch, D. and Yeh, G. S. Y. *J. Macromol. Sci. Phys.* 1973, **B7**, 121
23 Alexander, L. E., Ohlberg, S. and Russel, G. *J. Appl. Phys.* 1955, **26**, 1068
24 'Rubber Technology and Manufacture', 2nd Edn., (Eds. C. M. Blow and C. Hepburn), Butterworths, London, 1982
25 Mitchell, G. R. and Lovell, R. *Acta Crystallogr.* 1981, **A37**, 189
26 Treloar, L. R. G. *Trans. Faraday Soc.* 1947, **43**, 277, 284
27 Treloar, L. R. G. *Trans. Faraday Soc.* 1954, **50**, 881
28 Nobbs, J. H. and Bower, D. I. *Polymer* 1978, **19**, 1100
29 James, M. H. and Guth, E. *J. Chem. Phys.* 1947, **15**, 669
30 Flory, P. J. *Proc. Roy. Soc. London Ser. A* 1976, **351**, 351
31 Erman, B. and Flory, P. J. *Macromolecules* 1983, **16**, 1601
32 Flory, P. J. and Erman, B. *Macromolecules* 1982, **15**, 800
33 Flory, P. J. *J. Chem. Phys.* 1977, **66**, 5720
34 Tanaka, T. and Allen, G. *Macromolecules* 1977, **10**, 426
35 Jarry, J. P. and Monnerie, L. *Macromolecules* 1979, **12**, 316
36 Deloche, B. and Samulski, E. T. *Macromolecules* 1981, **14**, 575
37 Kilian, H. G. *Colloid Polym. Sci.* 1982, **260**, 895
38 Brown, D. J. and Windle, A. H. *J. Mater. Sci.* 1984, **18**, 1997, 2013, 2039
39 Yau, W. and Stein, R. S. *J. Polym. Sci. A-2* 1968, **6**, 1
40 Smith, K. J., Greene, A. and Ciferri, A. *Kolloid Z.* 1963, **194**, 49
41 Smith, K. J. and Puett, D. J. *J. Appl. Phys.* 1966, **37**, 346
42 De Candia, F., Romano, G., Russo, R. and Vittoria, V. *J. Polym. Sci. Polym. Phys. Edn.* 1982, **20**, 1525
43 Keller, A. and Machin, M. J. *J. Macromol. Sci. Phys.* 1967, **B1**, 41
44 Hill, M. J. and Keller, A. *J. Macromol. Sci. Phys.* 1969, **B3**, 153
45 Pick, M., Lovell, R. and Windle, A. H. *Polym.er* 1980, **21**, 1071
46 Flory, P. J. *J. Chem. Phys.* 1947, **15**, 397
47 Gaylord, R. J. *J. Polym. Sci. Polym. Phys. Edn.* 1976, **14**, 1827
48 Smith, K. J. *J. Polym. Sci. Polym. Phys. Edn.* 1983, **21**, 55
49 Ball, R. C., Doi, M., Edwards, S. F. and Warner, M. *Polymer* 1981, **22**, 1010
50 Graessley, W. W. *Adv. Polym. Sci.* 1974, **6**, 1
51 Mark, J. E. *Polym. Eng. Sci.* 1979, **19**, 254
52 Erman, B. and Flory, P. J. *Macromolecules* 1983, **16**, 1607
53 Kashiwagi, M., Folkes, M. J. and Ward, I. M. *Polymer* 1971, **12**, 697
54 Morgan, R. J. and Treoloar, L. R. G. *J. Polym. Sci. A-2* 1972, **10**, 51
55 Mitchell, G. R., Brown, D. J. and Windle, A. H. to be submitted to *Polymer*